

AKARI NEAR-INFRARED SPECTROSCOPY OF SDSS-SELECTED BLUE EARLY-TYPE GALAXIES

Joon Hyeop Lee ¹, Ho Seong Hwang ², Myung Gyoon Lee ³, Jong Chul Lee ³, and Hideo Matsuhara ⁴

¹*Korea Astronomy and Space Science Institute, Daejeon 305-348, Korea*

²*CEA Saclay/Service d'Astrophysique, F-91191 Gif-sur-Yvette, France*

³*Astronomy Program, Department of Physics and Astronomy, Seoul National University, Seoul 151-742, Korea*

⁴*Institute for Space and Astronautical Science, Japan Aerospace and Exploration Agency, Sagami-hara, Japan*

jhlee@astro.snu.ac.kr, hoseong.hwang@cea.fr, mglee@astro.snu.ac.kr,
jclee@astro.snu.ac.kr, maruma@ir.isas.jaxa.jp

ABSTRACT

A near-infrared (NIR; 2.5 – 4.5 μ m) spectroscopic survey of SDSS(Sloan Digital Sky Survey)-selected blue early-type galaxies (BEGs) has been conducted using the AKARI. The NIR spectra of 36 BEGs are secured, which are well balanced in their star-formation(SF)/Seyfert/LINER type composition. For high signal-to-noise ratio, we stack the BEG spectra all and in bins of several properties: color, specific star formation rate and optically-determined spectral type. We estimate the NIR continuum slope and the equivalent width of 3.29 μ m PAH emission. In the comparison between the estimated NIR spectral features of the BEGs and those of model galaxies, the BEGs seem to be old-SSP(Simple Stellar Population)-dominated metal-rich galaxies with moderate dust attenuation. The dust attenuation in the BEGs may originate from recent star formation or AGN activity and the BEGs have a clear feature of PAH emission, the evidence of current SF. BEGs show NIR features different from those of ULIRGs, from which we do not find any clear relationship between BEGs and ULIRGs. We find that Seyfert BEGs have more active SF than LINER BEGs, in spite of the fact that Seyferts show stronger AGN activity than LINERs. One possible scenario satisfying both our results and the AGN feedback is that SF, Seyfert and LINER BEGs form an evolutionary sequence: SF \rightarrow Seyfert \rightarrow LINER.

Subject headings: galaxies: elliptical and lenticular, cD — galaxies: evolution — galaxies: formation — galaxies: active

1. INTRODUCTION

Early-type galaxies are often regarded as the objects at the final stage of galaxy evolution. Throughout many observations, it has been revealed that most nearby early-type galaxies have red colors and very poor contents of cold gas (e.g. Faber & Gallagher 1976; Trager et al. 2000; Treu et al. 2006). Such observational evidence indicates that early-type galaxies are composed of old stars and that they probably will not have ad-

ditional star formation in the future. That is, most early-type galaxies seem to evolve *passively*, unlike late-type galaxies with active star formation.

However, since Abraham et al. (1999) and Menanteau et al. (1999) found a considerable fraction of early-type galaxies with blue colors and evidence of current star-formation in the Hubble Deep Field (Williams et al. 1996), the existence of *blue early-type galaxies* (hereafter, BEGs) has become a new important factor to be considered in the formation scenario of early-type galaxies.

BEGs are known to have positive color gradients (i.e. center bluer than outskirts) on average and consist of both old stars and young stars (Menanteau et al. 2001a; Elmegreen et al. 2005; Ferreras et al. 2005; Lee et al. 2006, 2008, 2010a). It has been also revealed that the internal color distributions of BEGs are neither homologous nor symmetric (Menanteau et al. 2004; Lee et al. 2006), and that some BEGs are suspected to host active galactic nuclei (AGNs) (Menanteau et al. 2005; Lee et al. 2006, 2008). Unlike typical red early-type galaxies (REGs) preferring high density environments, BEGs tend to reside in intermediate or low density environments (Kannappan et al. 2009; Lee et al. 2010b). The origin and future of BEGs are still controversial. Observational evidence indicates that some BEGs may originate from recent galaxy interaction or mergers (Lee et al. 2006), but the gas infall is also a possible mechanism to build BEGs (Menanteau et al. 2001b). After some time passes, BEGs may evolve into typical REGs (Lee et al. 2006, 2007, 2008), but it is also possible that they evolve into bulges of late-type galaxies (Hammer et al. 2005; Kannappan et al. 2009). In any case, BEGs are probably in the forming/growing phase of early-type galaxies or bulges.

To understand better the formation and evolution of BEGs, we need to inspect what happens in the inside of BEGs. Since more than a half of BEGs have evidence of their merger/interaction origin (Lee et al. 2006), the interaction-induced star formation (SF) is expected to make BEGs blue. On the other hand, galaxy merger/interaction sometimes also causes AGN activity (Kewley & Dopita 2003; Sánchez et al. 2005; Comerford et al. 2009), and the power-law continua of AGNs may affect the color of BEGs. Lee et al. (2008) reported that non-passive BEGs in the Sloan Digital Sky Survey (SDSS; York et al. 2000) include both SF galaxies and AGN host galaxies, the number ratio of which is about 3:5 for $-22.9 < {}^{0.1}M_r^1 < -20.7$. However, optical spectra are easily obscured by dust, causing the missing of a significant fraction of AGNs in optical surveys (Best et al. 2005). Moreover, ground-based spectroscopy (e.g. the SDSS spectroscopy) of bright

galaxies in the optical band often suffers the dilution of low-contrast emission lines due to strong emission lines (Ho et al. 1997), which also causes inaccuracy in estimating AGN activity.

One of the most powerful tools to probe the SF/AGN activity is the spectroscopy in the infrared (IR) band. Polycyclic aromatic hydrocarbons (PAHs; Sellgren 1984; Leger & Puget 1984) have been detected in various objects, such as HII region, protostellar clouds, planetary nebulae, and SF galaxies (Peeters et al. 2002; Hony 2002). It is known that UV photons excite the vibrational and stretching modes of PAH molecules, from the relaxation of which broad IR emission lines (such as 3.3, 6.2, 7.7, 8.6 and 11.2 μm lines) are produced (Cherchneff & Barker 1989; Shan et al. 1991). Such PAH emission features are good indicators of SF activity. On the other hand, Voit (1992) argued that PAHs in the central region of an AGN can be destructed by the strong X-ray emission from the AGN. Furthermore, AGN activity is known to suppress SF itself (AGN feedback; Antonuccio-Delogu & Silk 2008; Rafferty et al. 2008). Thus, those properties of PAH emission are believed to provide a reasonably clean diagnostic between SF and AGN. In addition, the shape of the IR continuum is another indicator of SF/AGN, because SF galaxies and AGNs have different spectral energy distribution (e.g. Imanishi et al. 2008; Risaliti et al. 2006, 2010). However, no systematic IR spectroscopic surveys of BEGs are seen in the literature.

In this paper, we report the result of the first BEG spectroscopic survey in the near-IR (NIR) band, using the AKARI (Murakami et al. 2007) InfraRed Camera (IRC; Onaka et al. 2007). The outline of this paper is as follows. Section 2 describes the target selection and the AKARI spectroscopic observation. Section 3 explains the reduction and analysis of the AKARI data. The extracted NIR spectra of BEGs and their features are shown in §4. The results are discussed in §5, and the main results and their implication are summarized in §6. Throughout this paper, we adopt the cosmological parameters: $h = 0.7$, $\Omega_\Lambda = 0.7$, and $\Omega_M = 0.3$.

¹Absolute Petrosian magnitude in the r band with K-correction as if the object were at $z = 0.1$ (Lee et al. 2008). All magnitudes in this paper are in the AB system.

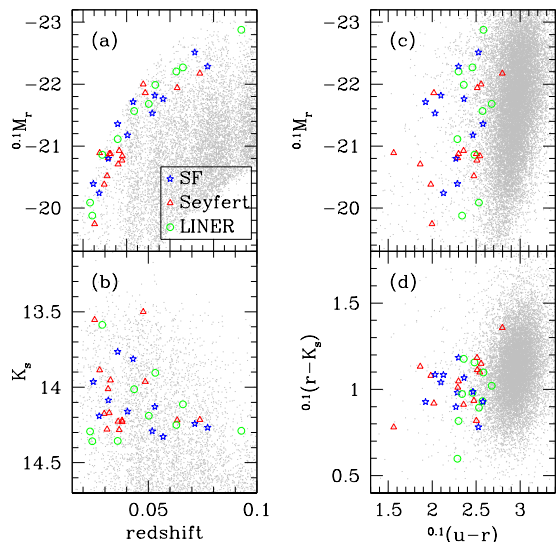


Fig. 1.— Basic optical-NIR properties of the observed 36 blue early-type galaxies (BEGs). (a) Absolute magnitude in the r band as a function of redshift; (b) Apparent magnitude in the K_s band as a function of redshift; (c) the color – magnitude relation; and (d) the color – color relation. The small dots are SDSS early-type galaxies and the large symbols are the BEGs: stars for star-forming (SF) BEGs, triangles for Seyfert BEGs and circles for LINER BEGs (classified in Fig. 2).

2. OBSERVATION

2.1. Target Selection

We selected 59 non-passive (i.e. currently star-forming or hosting an AGN) BEG targets based on the scheme of Lee et al. (2008), using the spectroscopic sample of galaxies in the SDSS Data Release 4 (DR4; Adelman-McCarthy et al. 2006). We adopted the physical parameters of the galaxies from several value-added galaxy catalogs (VAGCs) drawn from the SDSS: photometric parameters from the SDSS pipeline (Stoughton et al. 2002), structural parameters estimated by Park & Choi (2005) and Choi et al. (2007), and spectroscopic parameters from Max-Planck-Institute for Astrophysics (MPA) / Johns Hopkins University (JHU) VAGC (Kauffmann et al. 2003; Tremonti et al. 2004; Gallazzi et al. 2006). Firstly, we selected the early-type galaxies from the SDSS galaxies using

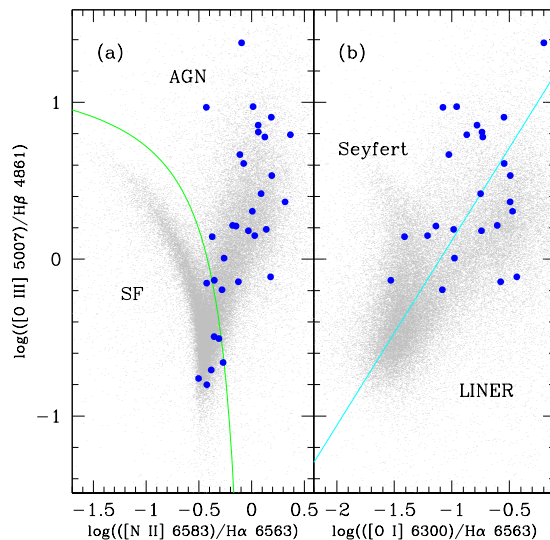


Fig. 2.— The distribution of SDSS early-type galaxies (small dots) and the BEGs (filled circle) in the line flux ratio diagram. (a) The line is the boundary dividing SF galaxies (lower-left) and AGNs (upper-right), given by Kauffmann et al. (2003). (b) The line is the boundary dividing Seyferts (upper-left) and LINERs (lower-right), given by Kewley et al. (2006). The number of filled circles is smaller than our BEG sample size, because the BEGs with each line S/N > 3 are plotted here. SF BEGs are not plotted in (b).

their distribution in the color, color gradient and light-concentration parameter space (Park & Choi 2005). Next, we divided the selected early-type galaxies into REGs and BEGs, using the method of Lee et al. (2006) based on the color distribution of bright early-type galaxies as a function of redshift². The BEGs were classified using their flux ratios between several spectral lines (e.g. BPT diagram; Baldwin et al. 1981; Kewley et al. 2006) into passive, SF, Seyfert, and low ionization nuclear emission region (LINER) galaxies, among which passive BEGs were excluded. Finally, we dropped BEGs with conspicuous sub-structures or disk components in visual checks. Among the BEGs selected in this scheme, we chose the target

²Here, BEGs are bluer than the Gaussian peak in the $(g-r)$ color distribution of the bright ($0.1M_r < -20$) early-type galaxies, by more than 3σ , where σ is the Gaussian spread.

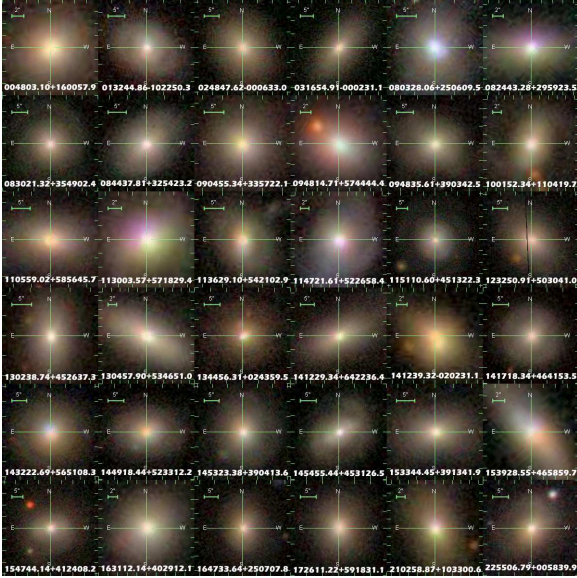


Fig. 3.— The atlas images of the observed 36 BEGs, retrieved from the SDSS. The bar in each image represents a scale of $2''$ or $5''$.

objects as non-passive BEGs at $0.02 < z < 0.1$ with $K_s < 14.4$ ³. The magnitude limit was applied to ensure the quality of the AKARI spectroscopy.

As a result, 59 BEGs were selected and proposed to be observed, but only 36 targets among them were successfully observed by the AKARI⁴. Fig. 1 shows the basic optical-NIR properties of the 36 BEGs in our sample: their magnitudes as a function of redshift, color – magnitude relation and color – color relation, confirming that our sample BEGs are blue and relatively bright objects. Fig. 2 displays the distribution of the BEGs in the line flux ratio diagrams, showing that the SF:Seyfert:LINER composition in our BEG sample is balanced well (11:15:10). In Fig. 3, the atlas images of the BEGs retrieved from the SDSS are presented. The basic properties of the BEGs are

³The ‘20 mag arcsec⁻² isophotal K_s fiducial ellipse aperture magnitude’ from the Two Micron All Sky Survey (2MASS; Jarrett et al. 2000) Extended Source Catalog (XSC). <http://www.ipac.caltech.edu/2mass/>.

⁴ There is various unpredictability in the space telescope operation, which makes it difficult to carry out the observations exactly as planned. Because of such unpredictability, the perfect success of proposed observations is not guaranteed.

summarized in Table 1.

2.2. AKARI Spectroscopy

The AKARI⁵ is a Japanese infrared astronomy satellite, from the Institute of Space and Astronautical Science (ISAS) of the Japanese Aerospace Exploration Agency (JAXA). It was launched on 21 February 2006 and ran out of its on-board coolant (Helium) supply on 26 August 2007 after its successful operation. The observation of our BEG targets was conducted during the AKARI open-time operation, the post-Helium phase of the AKARI observation, in which NIR ($1.8 - 5.5 \mu\text{m}$) imaging and spectroscopic observations are available.

The observation was conducted from November 2008 to August 2009. The target BEGs were observed using the IRCZ4 Astronomical Observing Template (AOT), which is the spectroscopic AOT of the IRC. Between the grism and prism, we selected the grism spectroscopy that has better spectroscopic resolution. The $1-\sigma$ noise equivalent flux density of the IRCZ4 grism is about 0.2 mJy , and its spectroscopic resolution is $R \sim 120$. As the target positioning option, we used the point source aperture (N_p), because the typical effective radius of target BEGs is only several arcseconds. Among the successfully-observed 36 targets, 29 objects were observed twice, while seven targets only once. The net exposure time for a single pointing observation is about six minutes (Onaka et al. 2007; Imanishi et al. 2008).

3. DATA REDUCTION AND ANALYSIS

3.1. Basic Data Reduction and Median Stacking

Unlike our expectation, two pointings per each object were not enough to secure sufficient signal-to-noise ratio (S/N) for most targets (a half of the spectra have $3.5 - 3.9 \mu\text{m}$ continua with $S/N < 6$), although the spectra of a few objects are relatively good. Thus, we applied the median stacking analysis technique for high S/N. The steps of the stacking analysis are as follows:

⁵http://www.ir.isas.jaxa.jp/ASTRO-F/Outreach/index_e.html

- Step.1 We used the *IRC Spectroscopy Toolkit for Phase 3 data Version 20090211* provided by the AKARI team, for the basic processes such as dark subtraction, image flat fielding, spectral flat fielding, image combining, source detection and extraction, sky subtraction, wavelength calibration and flux calibration.
- Step.2 Using the SDSS spectroscopic redshift, we converted the observer-frame wavelength into the rest-frame wavelength for each object. Since the rest-frame wavelength ranges are different between objects, we trimmed each spectrum with the rest-frame wavelength range of 2.5 – 4.5 μm .
- Step.3 All trimmed spectra were normalized for the median flux density at $3.5 < \lambda < 3.9 \mu\text{m}$ to be identical.
- Step.4 We stacked the normalized spectra by taking a median. We also produced several median-stacked spectra in bins of several properties such as optical spectral type, optical color, and [OII]-based specific star formation rate.

We selected the median stacking instead of mean stacking, because it removes unreal data points (hot or bad pixels) more effectively, whereas it improves data quality similarly to that the mean stacking does. Not only the total stacking (i.e. stacking all spectra into a single spectrum) but also subsample stacking was carried out to compare the NIR spectral features between subsamples with different optical properties. We simply estimated the uncertainty of the stacked spectra, by supposing that the spectral noise follows the Poisson error and that the S/N is accumulated during the stacking process. That is,

$$(S/N)_s = \sqrt{\sum (S/N)_i^2}, \quad (1)$$

where $(S/N)_s$ is the S/N of the stacked spectrum and $(S/N)_i$ is the S/N of the individual spectra.

3.2. Spectral Fitting

We used the power law continuum + 3.29 μm PAH emission (Gaussian) formula (Risaliti et al. 2006) to fit the stacked spectra:

$$F_\lambda = A\lambda^\Gamma + B e^{-\frac{(\lambda-3.29\mu\text{m})^2}{2\sigma^2}}, \quad (2)$$

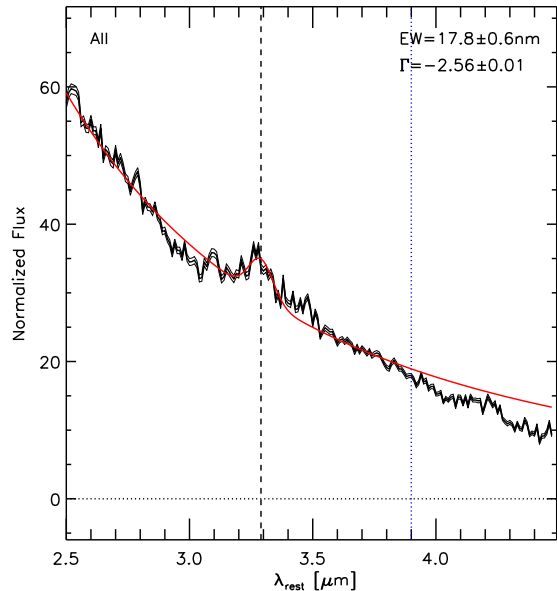


Fig. 4.— The stacked spectrum (noisy thick solid line) using all BEGs in our sample. The noisy thin solid lines show the S/N-accumulated noise and the smooth solid line is the continuum + PAH emission fit using Equation (2). The estimated PAH equivalent width ($EW_{3.29}$) and the continuum slope (Γ) are denoted on the upper-right corner. The dashed vertical line shows the PAH central wavelength (3.29 μm), and the dotted vertical line shows the upper limit of the wavelength range for fitting (3.9 μm).

where F_λ is the flux density, λ is the wavelength in unit of μm , Γ is the continuum slope, σ is the Gaussian spread in unit of μm , and A and B are amplitudes. The fitting was conducted in the wavelength range of 2.5 – 3.9 μm , because the Br α emission and CO absorption lines may affect the NIR spectra significantly at $\lambda > 4\mu\text{m}$ (Imanishi et al. 2008; Risaliti et al. 2010).

4. RESULTS

Fig. 4 displays the stacked spectrum of all BEGs in our sample. In this spectrum, a clear PAH emission line is found, the central wavelength of which is 3.29 μm . The continuum is overall fit well to the function in the fitting range (2.5 – 3.9 μm). The ice-cored dust absorption ($\lambda \sim$

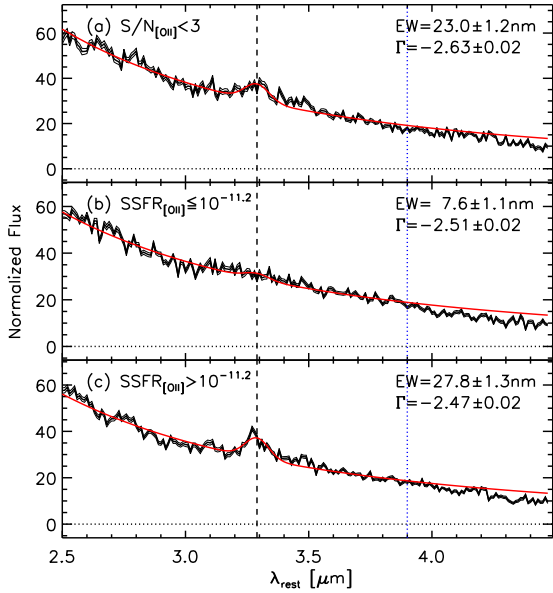


Fig. 5.— The stacked spectra of BEGs in three subsamples with different [OII]-based specific star formation rates (SSFRs). (a) $S/N_{[\text{OII}]} < 3$ (that is, $\text{SSFR}_{[\text{OII}]}$ is not available); and among the BEGs with $S/N_{[\text{OII}]} \geq 3$: (b) $\text{SSFR}_{[\text{OII}]} \leq 6.3$ and (c) $\text{SSFR}_{[\text{OII}]} > 6.3$, in unit of 10^{-12} yr^{-1} .

$2.8 - 3.2 \mu\text{m}$) feature is marginally found, but the bare carbonaceous dust absorption ($\lambda \sim 3.4 \mu\text{m}$) feature is hardly seen in Fig. 4. Around $\lambda \sim 3.4 \mu\text{m}$, instead of absorption features, a marginal excess is seen, which we currently have no idea of. It is noted that the long-ward of $3.9 \mu\text{m}$ of the stacked spectrum shows values totally lower than the fit. The known line features at $\lambda > 4 \mu\text{m}$ is $\text{Br}\alpha$ emission ($\lambda = 4.05 \mu\text{m}$) and CO_2 absorption ($\lambda = 4.26 \mu\text{m}$), but those features are not clearly identified in Fig. 4. The apparent ‘dip’ at $\lambda > 4 \mu\text{m}$ may be simply because the spectral fitting was carried out in the wavelength range of $2.5 - 3.9 \mu\text{m}$.

Figs. 5 – 7 show the stacked spectra of the BEGs in bins of several properties: [OII]-based specific star formation rate ($\text{SSFR}_{[\text{OII}]}$), $^{0.1}(u-r)$ color, and optical spectral type. In the estimation of SSFR, the star formation rate (SFR) was estimated using the [OII] emission line that is known to be hardly contaminated by AGN emission (Ho 2005; Kim et al. 2006), and the stellar mass was derived using the 2MASS K_s magni-

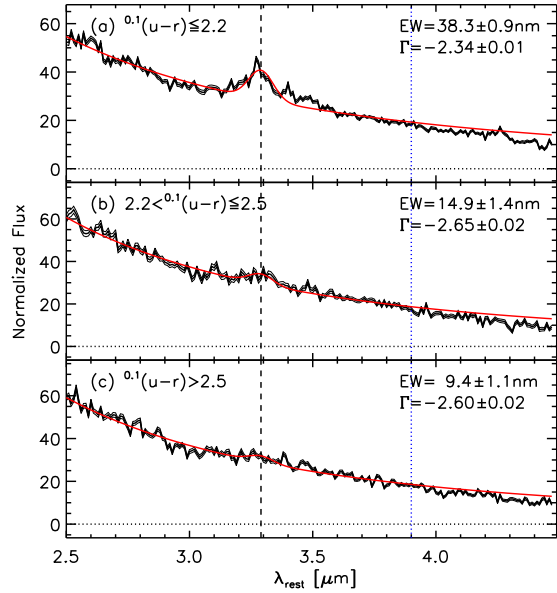


Fig. 6.— The stacked spectra of BEGs in three subsamples with different optical colors. (a) $^{0.1}(u-r) \leq 2.2$, (b) $2.2 < ^{0.1}(u-r) \leq 2.5$ and (c) $^{0.1}(u-r) > 2.5$.

tude (see Lee et al. 2010a). When considering the objects with sufficient [OII] emission signal ($S/N_{[\text{OII}]} \geq 3$; Fig. 5b and Fig. 5c), PAH emission is hardly found for low $\text{SSFR}_{[\text{OII}]}$ BEGs, whereas the stacked spectrum of the high $\text{SSFR}_{[\text{OII}]}$ BEGs shows a clear PAH emission feature. This confirms the fact that PAH emission reflects current SF. It is noted that 14 BEGs have low $S/N_{[\text{OII}]}$, which may be mainly due to the difficulty in measuring the [OII](3727Å) line using the SDSS spectroscopy (3800 – 9200Å) at low redshift.

Fig. 6 shows that the bluer BEGs have the stronger PAH emission feature, which indicates that the blue colors of BEGs reflect their SF activity. This trend is also confirmed in Fig. 7: the PAH equivalent width ($\text{EW}_{3.29}$) of SF BEGs (25.2 nm) is larger than those of Seyfert and LINER BEGs (17.2 nm and 13.4 nm, respectively). In Fig. 7, it is noted that the $\text{EW}_{3.29}$ of Seyfert BEGs (17.2 ± 0.8 nm) is larger than that of LINER BEGs (13.4 ± 1.4 nm) by more than 2σ . Seyferts show stronger AGN activity than LINERs (e.g. Groves et al. 2006) and the current consensus on the relationship between AGN activity and PAH/SF is that

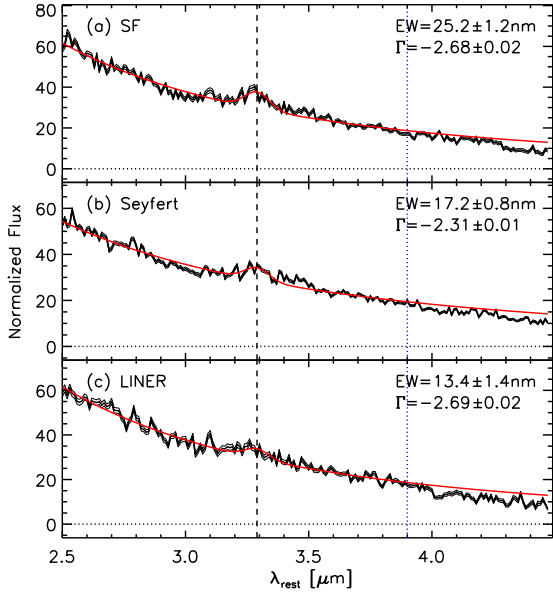


Fig. 7.— The stacked spectra of BEGs in three subsamples with different optical spectral types. (a) SF BEGs, (b) Seyfert BEGs and (c) LINER BEGs.

AGN activity destroys PAH particles and suppresses SF (Voit 1992; Antonuccio-Delogu & Silk 2008; Rafferty et al. 2008). Apparently, however, our results seem to be contradictory to such previous understanding (i.e. Seyfert BEGs are more active than LINER BEGs in both AGN and SF activity).

5. DISCUSSION

5.1. The Identity of BEGs from the AKARI View

BEGs are known to have not only very young stars but also a considerable amount of old stars (Menanteau et al. 2001a; Ferreras et al. 2005; Lee et al. 2010a). In our results, however, it is not easy to check this previous knowledge independently, because the NIR continuum slope (Γ) depends on both stellar and dust contents (dust either in host galaxies or in AGN tori). Fig. 8 shows the variation of Γ as a function of age, metallicity, star formation history and dust attenuation, using the models of Bruzual & Charlot (2003): simple stellar population (SSP), exponentially-decreasing

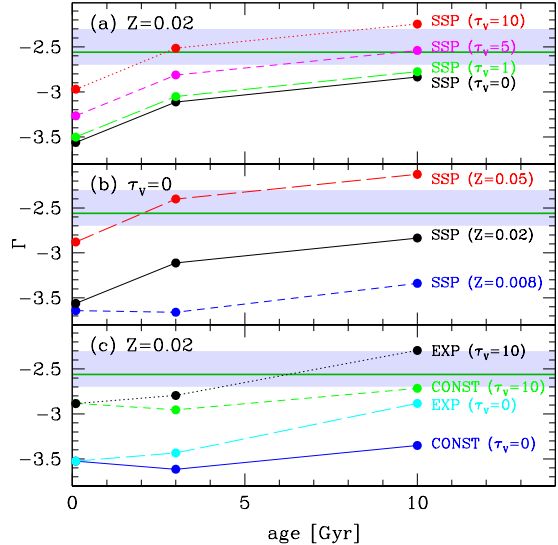


Fig. 8.— Comparison of NIR continuum slope (Γ) between population synthesis models and the stacked spectra of BEGs: (a) the simple stellar population (SSP) models with solar metallicity ($Z=0.02$) and various dust attenuation values (solid, long-dashed, short-dashed and dotted lines for $\tau_V = 0, 1, 5$ and 10 , where τ_V is the dust optical depth in the V band); (b) the SSP models with $\tau_V = 0$ and various metallicity (short-dashed, solid and long-dashed lines for $Z=0.008, 0.02$ and 0.05); and (c) the exponentially-decreasing star formation rate model with the exponential time scale of 1 Gyr (EXP; long-dashed and dotted lines for $\tau_V = 0$ and 10) and the model with constant star formation rate of $1 M_\odot/\text{yr}$ (CONST; solid and short-dashed lines for $\tau_V = 0$ and 10), with $Z=0.02$. The shaded area shows the Γ range of the BEG stacked spectra and the horizontal solid line shows the Γ value of the all-BEG-stacked spectrum. Dust attenuation was estimated using the simple model of Charlot & Fall (2000).

and constant star formation rate models. In Fig. 8, it is found that Γ becomes less negative as star formation ended earlier, as age increases, as metallicity increases and as dust increases. Due to this degeneracy, it is difficult to tell the dominant factor in determining Γ of BEGs. Even if we suppose that the NIR continuum of the BEGs is old-SSP-dominated from the previous knowledge (the age of most stars in BEGs is about 10 Gyr;

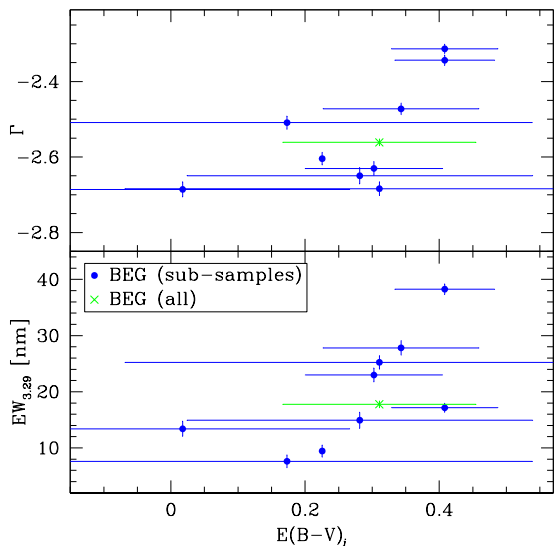


Fig. 9.— The internal extinction $E(B-V)_i$ versus the Γ and $EW_{3.29}$ of the BEGs. Filled circles are the values from the subsample-stacked spectra and cross is the value from the all-BEGs-stacked spectrum. The horizontal errorbars indicate the sample inter-quartile range for the median $E(B-V)_i$ value in each subsample.

e.g. Ferreras et al. 2005; Lee et al. 2010a), the Γ of the BEGs can be reproduced using either the metal-rich SSP model without dust or the significantly dust-attenuated SSP model with solar metallicity.

The effect of internal dust extinction is independently checked using the information extracted from the SDSS data; that is, using the Balmer decrement. Based on the formula of Calzetti et al. (1994), we derived the internal reddening $E(B-V)_i$ (median value for each subsample) and compared them with the Γ and $EW_{3.29}$ of the stacked BEGs in Fig. 9. It is found that the NIR spectral parameters have correlations with $E(B-V)_i$, in the sense that the Γ and $EW_{3.29}$ increase with increasing $E(B-V)_i$. The $E(B-V)_i$ values of the BEGs are not small, but seem to be not large enough to explain the Γ of the BEGs in Fig. 8 (the τ_V corresponding to $E(B-V) = 0.4$ is 1.14; De Ruyter et al. 2005). Thus, if we suppose moderate (not too strong) dust attenuation in the BEGs, Fig. 8 indicates that the BEGs may

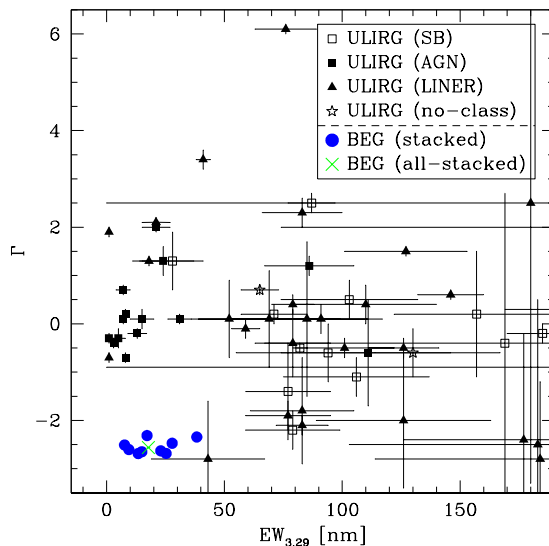


Fig. 10.— Comparison between BEGs and other objects in the $\Gamma - EW_{3.29}$ plane. The data for starburst ULIRGs (SB ULIRGs; open rectangles), AGN ULIRGs (filled rectangles), LINER ULIRGs (filled triangles) and not-classified ULIRGs (open stars) are from Risaliti et al. (2010). The filled circles are BEGs stacked in bins of several properties and the cross shows the all-BEGs-stacked result.

have stellar populations with slightly high metallicity, although this estimation is strongly model-dependent.

Meanwhile, BEGs are often thought to be the intermediate objects transforming from interacting galaxies or mergers to red elliptical galaxies or bulges of late-type galaxies (Lee et al. 2006, 2008; Kannappan et al. 2009). Known to have similar origins are Ultra-Luminous InfraRed Galaxies (ULIRGs). ULIRGs are very luminous in the IR band due to vigorous starburst and/or AGN activity (Veilleux et al. 1995, 1999a), and are thought to be formed by strong interaction or merger of two disk galaxies (Sanders et al. 1988). Risaliti et al. (2006, 2010) estimated the Γ and $EW_{3.29}$ of some ULIRGs, showing an interesting division between AGN-host ULIRGs and starburst ULIRGs.

Fig. 10 shows the loci of our BEGs on the $\Gamma - EW_{3.29}$ plane, compared with the objects presented in Risaliti et al. (2010). In this figure, it

is found that our BEGs have Γ and $EW_{3.29}$ values distinct from those of the ULIRGs, in the sense that the BEGs have largely negative Γ values (~ -2.5), while those of the ULIRGs are mostly larger than -2 (up to 6). The $EW_{3.29}$ of the BEGs is smaller than that of the ULIRGs on average, showing that the SF in the BEGs is not as active as that in the ULIRGs. The Γ value is expected to be largely positive when the NIR continuum is dominated by dust emission. In our BEG sample, however, even the stacked spectra using optical AGN or optical SF BEGs has largely negative Γ . This indicates that the dust amount in those BEGs may not be as large as that in ULIRGs, as shown already using the internal dust reddening derived from Balmer decrement (the mean $E(B - V)$ value of ULIRGs is larger than 1.0; Veilleux et al. 1999a,b).

In short, the Γ and $EW_{3.29}$ features of the BEGs are not easy to interpret, because they are affected by the combined effects of age, metallicity, star formation history and dust attenuation. However, based on some previous knowledge, Balmer line information and a few assumptions, the BEGs are thought to be old-SSP-dominated metal-rich galaxies with moderate dust attenuation. The dust attenuation in the BEGs may originate from recent star formation or AGN activity. This interpretation is consistent with the previous understanding of stellar populations in BEGs (that is, mostly old stars + partially young stars; Ferreras et al. 2005; Lee et al. 2010a). There is a possibility that ULIRGs are the progenitors of BEGs in the merging/interacting phase (Veilleux et al. 2002), but any clear evidence of the close relationship between BEGs and ULIRGs is not yet found in our results based on the NIR spectroscopy.

5.2. NIR Features and AGN Activity in BEGs

As introduced in §1, NIR spectroscopy provides interesting clues to the internal evolutionary process of the BEGs, related to their SF or AGN activity. Those clues become more useful when combined with the optical properties of the BEGs. Fig. 11 compares the stacked spectra in bins of several properties on the $\Gamma - EW_{3.29}$ plane, giving a summary of the key results in Fig. 4 – 7. The $EW_{3.29}$ reflects the current SF of the BEGs

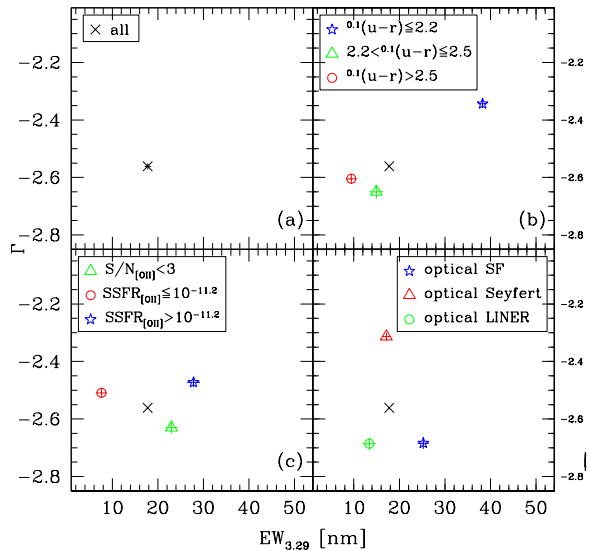


Fig. 11.— The Γ versus $EW_{3.29}$ of the BEGs stacked in bins of several properties: (a) all, (b) $0.1(u-r)$ color, (c) $SSFR_{[OIII]}$ and (d) optical spectral type. In every panel, the all-BEGs-stacked result is denoted as a cross.

well (Fig. 11c), but it is noted that the Seyfert BEGs have $EW_{3.29}$ larger than that of the LINER BEGs. As mentioned at the end of §4, this result is not well explained simply by the current consensus that AGN activity destroys PAH particles.

In addition to $EW_{3.29}$, another key parameter is Γ . As shown in Fig. 8, Γ is affected commonly by age, metallicity and dust. However, the bluest BEGs with the largest (least negative) Γ in Fig. 11b is not easily understood by the age or metallicity effects, because blue galaxies tend to be young or metal-poor, which will make Γ more negative unlike the bluest BEGs. Thus, the Γ difference between the bluest BEGs and the other BEGs seems to be mainly due to the difference in their dust contents. It is also noted that the optical SF BEGs have small (largely negative) Γ in Fig. 11d, which shows good consistency with the star formation history dependence of Γ , indicating that those SF BEGs are not very dusty. That is, several AGNs with dusty tori in the bluest BEG subsample seem to mainly contribute to the largest (least negative) Γ .

In Fig. 11c, the BEGs with large $SSFR_{[OIII]}$

have Γ intermediate between those of the bluest BEGs and optical SF BEGs. These are because the optical color, SSFR and optical spectral type of the BEGs do not tightly correlate: some non-SF BEGs have large $\text{SSFR}_{[\text{OII}]}$ or blue $^{0.1}(u-r)$ color. These results lead us again to the conclusion that the SF and the AGN activity in BEGs are not necessarily contradictory to each other. The coexistence of SF and AGN is not entirely new discovery (e.g. Tzanavaris & Georgantopoulos 2007; Treister et al. 2009), but currently it is widely believed that AGN activity tends to destroy PAH particles and to truncate SF (Voit 1992; Weinmann et al. 2006; Schwanski et al. 2007; Tortora et al. 2009). In our result, however, Seyfert BEGs have larger $\text{EW}_{3.29}$ than LINER BEGs, in spite of the fact that Seyferts show stronger AGN activity than LINERS.

This result may be explained by various ways. Smith et al. (2007) and Imanishi et al. (2008) showed that PAHs can survive even if they are close to AGNs when the AGNs are not dust-free, which gives an answer to how the AGN activity and PAH emission coexist. However, it does not sufficiently explain why stronger AGNs have stronger PAH emission features. One possibility is that Seyfert BEGs and LINER BEGs may not be the separate branches in BEG evolution. Satisfying our results, one possible scenario of BEG evolution is as follows (see also Lee et al. 2010a):

- Ph.1 SF BEG phase. Triggered by some mechanisms (possibly interaction or merger; Lee et al. 2006), active (but not very dusty) SF occurs in the progenitor of a BEG, originally consisting of old stars in the main. The NIR continuum is very similar to that of old passive galaxies, but the PAH emission is clearly detected.
- Ph.2 Seyfert BEG phase. After the central black hole in a BEG increases its mass by gas accretion, AGN activity starts. The SF in the BEG starts to be suppressed by the AGN feedback, but at this time, both AGN and SF activities coexist. The NIR continuum is contaminated by the AGN (Γ increases), and the PAH emission becomes weaker than that of SF BEGs.
- Ph.3 LINER BEG phase. The AGN feedback has truncated most SF by removing ambient gas

in the BEG. Since this makes the gas accretion into the central black hole stop also, AGN activity becomes weak as a natural result. The NIR continuum is intermediate between SF BEGs and Seyfert BEGs, and the PAH emission feature is weakest among the three phases.

After these three phases, the BEGs may evolve into REGs or bulges of late-type galaxies via the phase of passive BEGs (Lee et al. 2006, 2008; Kannappan et al. 2009). The proposed scenario is consistent with the findings about the relationship between Seyferts and LINERS in several recent studies (Schwanski et al. 2007, 2009; Hickox et al. 2009; Lee et al. 2010a).

6. SUMMARY

We conducted an AKARI NIR spectroscopic survey of SDSS-selected BEGs. We secured the NIR spectra of 36 BEGs that are well balanced in their SF/Seyfert/LINER composition. We stacked the BEG spectra all and in bins of several properties, such as color, SSFR and optical spectral type. This is the first presentation of the BEG NIR (2.5 – 4.5 μm) spectra, from which we estimated the NIR continuum slope (Γ) and the equivalent width of 3.29 μm PAH emission ($\text{EW}_{3.29}$).

In the comparison between the estimated NIR spectral features of the BEGs and those of the model galaxies, the BEGs seem to be old-SSP-dominated metal-rich galaxies with moderate dust attenuation. The dust attenuation in the BEGs may originate from recent star formation or AGN activity and the BEGs have a clear feature of PAH emission, the evidence of current SF. BEGs show NIR features different from those of ULIRGs, from which we can not find any clear relationship between BEGs and ULIRGs.

We compared the stacked spectra of the BEGs in bins of several properties, confirming that the PAH emission is a good indicator of current SF. We found that Seyfert BEGs have more active SF than LINER BEGs, in spite of the fact that the AGN activity in Seyfert BEGs are stronger than that in LINER BEGs. One possible scenario satisfying both this result and the AGN feedback is that SF, Seyfert and LINER BEGs form an evolutionary sequence: SF \rightarrow Seyfert \rightarrow LINER.

JHL is a member of the Dedicated Researchers for Extragalactic AstronoMy (DREAM) in Korea Astronomy and Space Science Institute (KASI). This paper is based on the data produced in the AKARI open-time phase-3 project, *Infrared Spectroscopy of Blue Early-type Galaxies* (ISBEG; PI: JHL). The AKARI is a JAXA project with the participation of ESA. The authors appreciate the help and support of the all AKARI project members. The authors are grateful to an anonymous referee for useful comments. This work was supported by the National Research Foundation of Korea (NRF) grant funded by the Korea Government (MEST) (No. R01-2007-000-20336-0). Funding for the SDSS and SDSS-II has been provided by the Alfred P. Sloan Foundation, the Participating Institutions, the National Science Foundation, the US Department of Energy, the National Aeronautics and Space Administration, the Japanese Monbukagakusho, the Max Planck Society, and the Higher Education Funding Council for England. The SDSS Web site is <http://www.sdss.org/>. The SDSS is managed by the Astrophysical Research Consortium for the Participating Institutions. The Participating Institutions are the American Museum of Natural History, Astrophysical Institute Potsdam, the University of Basel, the University of Cambridge, Case Western Reserve University, the University of Chicago, Drexel University, Fermilab, the Institute for Advanced Study, the Japan Participation Group, Johns Hopkins University, the Joint Institute for Nuclear Astrophysics, the Kavli Institute for Particle Astrophysics and Cosmology, the Korean Scientist Group, the Chinese Academe of Sciences (LAMOST), Los Alamos National Laboratory, the Max-Planck-Institute for Astronomy (MPIA), the Max Planck Institute for Astrophysics (MPA), New Mexico State University, Ohio State University, the University of Pittsburgh, the University of Portsmouth, Princeton University, the US Naval Observatory, and the University of Washington. This publication makes use of data products from the 2MASS, which is a joint project of the University of Massachusetts and the Infrared Processing and Analysis Center/California Institute of Technology, funded by the National Aeronautics and Space Administration and the National Science Foundation.

REFERENCES

- Abraham, R. G., Ellis, R. S., Fabian, A. C., Tanvir, N. R., & Glazebrook, K. 1999, *MNRAS*, 303, 641
- Adelman-McCarthy, J., et al. 2006, *ApJS*, 162, 38
- Antonuccio-Delogu, V., & Silk, J. 2008, *MNRAS*, 389, 1750
- Baldwin, J. A., Phillips, M. M., & Terlevich, R. 1981, *PASP*, 93, 5
- Best, P. N., Kauffmann, G., Heckman, T. M., Brinchmann, J., Charlot, S., Ivezić, Ž., & White, S. D. M. 2005, *MNRAS*, 362, 25
- Bruzual, G., & Charlot, S. 2003, *MNRAS*, 344, 1000
- Calzetti, D., Kinney, A. L., & Storchi-Bergmann, T. 1994, *ApJ*, 429, 582
- Charlot, S., & Fall, S. M. 2000, *ApJ*, 539, 718
- Cherchneff, I. & Barker, J. R. 1989, *ApJ*, 341, L21
- Choi, Y.-Y., Park, C., & Vogeley, M. S. 2007, *ApJ*, 658, 884
- Comerford, J. M., et al. 2009, *ApJ*, 698, 956
- Elmegreen, D. M., Elmegreen, B. G., & Ferguson, T. E. 2005, *ApJ*, 623, L71
- Faber, S. M., & Gallagher, J. S. 1976, *ApJ*, 204, 365
- Ferreras, I., Lisker, T., Carollo, M., & Lilly, S. J. 2005, *ApJ*, 635, 243
- Gallazzi, A., et al. 2006, *MNRAS*, 370, 1106
- Groves, B., Kewley, L., Kauffmann, G., & Heckman, T. 2006, *New Astronomy Reviews*, 50, 743
- Hammer, F., Flores, H., Elbaz, D., Zheng, X. Z., Liang, Y. C., & Cesarsky, C. 2005, *A&A*, 430, 115
- Hickox, R. C., et al. 2009, *ApJ*, 696, 891
- Ho, L. C. 2005, *ApJ*, 629, 680
- Ho, L. C., Filippenko, A. V., & Sargent, W. L. W. 1997, *ApJS*, 112, 315

- Hony, S. 2002, Ph.D. thesis, University of Amsterdam
- Imanishi, M., Nakagawa, T., Ohya, Y., Shirahata, M., Wada, T., Onaka, T., & Oi, N. 2008, PASJ, 60, 489
- Jarrett, T. H., Chester, T., Cutri, R., Schneider, S., Rosenberg, J., Huchra, J. P., & Mader, J. 2000, AJ, 120, 298
- Kannappan, S. J., Guie, J. M., & Baker, A. J. 2009, AJ, 138, 579
- Kauffmann, G., et al. 2003, MNRAS, 341, 33
- Kewley, L. J. & Dopita, M. A. 2003, RevMexAA, 17, 83
- Kewley, L. J., Groves, B., Kauffmann, G., Heckman, T. 2006, MNRAS, 372, 961
- Kim, M., Ho, L. C., & Im, M. 2006, ApJ, 642, 702
- Lee, J. H., Lee, M. G., & Hwang, H. S. 2006, ApJ, 650, 148
- Lee, J. H., Lee, M. G., Kim, T. H., Hwang, H. S., Park, C., & Choi, Y.-Y. 2007, ApJ, 663, L69
- Lee, J. H., Lee, M. G., Park, C., & Choi, Y.-Y. 2008, MNRAS, 389, 1791
- Lee, J. H., Lee, M. G., Park, C., & Choi, Y.-Y. 2010a, MNRAS, 401, 1804
- Lee, J. H., Lee, M. G., Park, C., & Choi, Y.-Y. 2010b, MNRAS, in press (arXiv:0911.4386)
- Leger, A., & Puget, J. L. 1984, A&A, 137, L5
- Menanteau, F., Abraham, R. G., & Ellis, R. S. 2001a, MNRAS, 322, 1
- Menanteau, F., Ellis, R., Abraham, R., Berger, A., & Cowie, L. 1999, MNRAS, 309, 208
- Menanteau, F., Jimenez, R., & Matteucci, F. 2001b, ApJ, 562, L23
- Menanteau, F., et al. 2004, ApJ, 612, 202
- Menanteau, F., et al. 2005, ApJ, 620, 697
- Murakami, H., et al. 2007, PASJ, 59, 369
- Onaka, T., et al. 2007, PASJ, 59, 401
- Park, C., & Choi, Y.-Y. 2005, ApJ, 635, L29
- Peeters, E., Hon, S., Van Kerckhoven, C., Tielens, A. G. G. M., Allamandola, L. J., Hudgins, D. M., & Bauschlicher, C. W. 2002, A&A, 390, 1089
- Rafferty, D. A., McNamara, B. R., & Nulsen, P. E. J. 2008, ApJ, 687, 899
- Risaliti, G., Imanishi, M., & Sani, E. 2010, MNRAS, 401, 197
- Risaliti, G., et al. 2006, MNRAS, 365, 303
- De Ruyter, S., Van Winckel, H. Dominik, C., Waters, L. B. F. M., & Dejonghe, H. A&A, 161, 166
- Sanders, D. B., Soifer, B. T., Elias, J. H., Madore, B. F., Matthews, K., Neugebauer, G., & Scoville, N. Z. 1988 ApJ, 325, 74
- Sánchez, S. F., Becker, T., Garcia-Lorenzo, B., Benn, C. R., Christensen, L., Kelz, A., Jahnke, K., & Roth, M. M. 2005, A&A, 429, L21
- Sellgren, K. 1984, ApJ, 277, 623
- Schawinski, K., Thomas, D., Sarzi, M., Maraston, C., Kaviraj, S., Joo, S.-J., Yi, S. K., & Silk, J. 2007, MNRAS, 382, 1415
- Schawinski, K., et al. 2009, ApJ, 690, 1672
- Shan, J., Sutton, M. & Lee, L. C. 1991, ApJ, 383, 459
- Smith, J. D. T., et al. 2007, ApJ, 656, 770
- Stoughton, C., et al. 2002, AJ, 123, 485
- Trager, S. C., Faber, S. M., Worthey, Guy, & González, J. J. 2000, AJ, 119, 1645
- Tortora, C., Antonuccio-Delogu, V., Kaviraj, S., Silk, J., Romeo, A. D., & Becciani, U. 2009, MNRAS, 396, 61
- Treister, E., et al. 2009, ApJ, 706, 535
- Tremonti, C. A., et al. 2004, ApJ, 613, 898
- Treu, T., Koopmans, L. V., Bolton, A. S., Burles, S., & Moustakas, L. A. 2006, ApJ, 640, 662
- Tzanavaris, P., & Georgantopoulos, I. 2007, A&A, 468, 129

- Veilleux, S., Kim, D.-C., Sanders, D. B., Mazarrella, J. M., & Soifer, B. T. 1995, *ApJS*, 98, 171
- Veilleux, S., Kim, D.-C., & Sanders, D. B. 2002, *ApJS*, 143, 315
- Veilleux, S., Sanders, D. B., & Kim, D.-C. 1999a, *ApJ*, 522, 113
- Veilleux, S., Sanders, D. B., & Kim, D.-C. 1999b, *ApJ*, 522, 139
- Voit, G. M. 1992, *MNRAS*, 258, 841
- Weinmann, S. M., van den Bosch, F. C., Yang, X., Mo, H. J., Croton, D. J., & Moore, B. 2006, *MNRAS*, 372, 1161
- Williams, R. E., et al. 1996, *AJ*, 112, 1335
- York, D. G., et al. 2000, *AJ*, 120, 1579

TABLE 1
BASIC PROPERTIES OF THE BEGs

SDSS ID	Redshift	$^{0.1}M_r$ (1)	K_s (2)	Optical Spectral Type	$^{0.1}(u-r)$	SSFR _[OII] (3)
004803.10+160057.9	0.050	-21.681	14.189	LINER	2.676	0.000
013244.86-102250.3	0.032	-20.876	14.171	Seyfert	2.503	—
024847.62-000633.0	0.025	-20.392	13.964	SF	2.287	—
031654.91-000231.1	0.023	-20.087	14.293	LINER	2.532	—
080328.06+250609.5	0.028	-20.888	13.886	Seyfert	1.563	—
082443.28+295923.5	0.025	-19.743	13.553	Seyfert	1.998	—
083021.32+354902.4	0.053	-21.818	14.129	SF	2.099	11.989
084437.81+325423.2	0.032	-20.808	14.011	Seyfert	2.290	25.838
090455.34+335722.1	0.044	-21.566	14.013	LINER	2.572	0.306
094814.71+574444.4	0.030	-20.382	14.175	Seyfert	1.984	—
094835.61+390342.5	0.071	-22.515	14.242	SF	2.526	—
100152.34+110419.7	0.052	-21.531	14.291	SF	2.033	14.902
110559.02+585645.7	0.048	-21.997	13.501	Seyfert	2.557	1.804
113003.57+571829.4	0.036	-20.708	14.227	Seyfert	1.863	37.973
113629.10+542102.9	0.063	-21.939	14.218	Seyfert	2.513	9.908
114721.61+522658.4	0.049	-21.858	13.964	Seyfert	2.019	55.042
115110.60+451322.3	0.036	-21.113	14.356	LINER	2.287	2.687
123250.91+503041.0	0.063	-22.204	14.250	LINER	2.299	6.698
130238.74+452637.3	0.024	-19.878	14.358	LINER	2.340	—
130457.90+534651.0	0.029	-20.859	13.587	LINER	2.481	0.014
134456.31+024359.5	0.077	-22.287	14.267	SF	2.299	—
141229.34+642236.4	0.036	-21.358	13.765	SF	2.578	—
141239.32-020231.1	0.074	-22.175	14.215	Seyfert	2.798	—
141718.34+464153.5	0.038	-20.839	14.229	Seyfert	2.542	1.952
143222.69+565108.3	0.043	-21.713	13.813	SF	1.925	9.136
144918.44+523312.2	0.066	-22.270	14.113	LINER	2.457	3.405
145323.38+390413.6	0.032	-20.798	14.086	SF	2.270	—
145455.44+453126.5	0.037	-20.924	14.283	Seyfert	2.356	0.000
153344.45+391341.9	0.040	-21.176	14.160	SF	2.463	0.365
153928.55+465859.7	0.038	-20.770	14.220	Seyfert	2.509	—
154744.14+412408.2	0.033	-20.873	13.954	Seyfert	2.299	35.112
163112.14+402912.1	0.031	-20.516	14.279	Seyfert	2.476	—
164733.64+250707.8	0.057	-21.762	14.328	SF	2.363	6.926
172611.22+591831.1	0.027	-20.241	14.191	SF	2.128	—
210258.87+103300.6	0.093	-22.877	14.289	LINER	2.583	0.193
225506.79+005839.9	0.053	-21.988	13.905	LINER	2.359	0.046

NOTE.—(1) The r -band absolute magnitude with K-correction (Petrosian magnitude), (2) the K_s -band apparent magnitude (20 mag arcsec⁻² isophotal K_s fiducial ellipse aperture magnitude), and (3) the specific star formation rate in unit of 10^{-12} yr⁻¹ (that is, the newly-forming stellar mass per unit stellar mass per year). For the objects with $S/N_{[\text{OII}]} < 3$, their SSFRs were not estimated (—).